Role of Y Admixture in $(Lu_{1-x}Y_x)_3Al_5O_{12}$:Pr Ceramic Scintillators Free of Host Luminescence

Chen Hu,[1] Xiqi Feng,[1] Jiang Li,[1,*] Anna Vedda,[2] Dongzhou Ding,[1] Zhenzhen Zhou,[1] Huamin Kou,[1,†] and Yubai Pan[1]

[1]*Key Laboratory of Transparent Opto-functional Inorganic Materials, Shanghai Institute of Ceramics, Chinese Academy of Sciences, Shanghai 200050, China*

[2]*Department of Materials Science, University of Milano-Bicocca, Via Cozzi 55, 20125 Milano, Italy*

(Received 23 May 2016; revised manuscript received 13 November 2016; published 30 December 2016)

Point defects can seriously affect the performance of scintillator materials. Therefore, the fabrication of defect-free scintillators is an exciting goal for materials scientists. By applying an advanced optical ceramic preparation process, $(Lu_{1-x}Y_x)_3Al_5O_{12}$:Pr (LuYAG:Pr) ceramics free of defect-induced host luminescence are produced. Moreover, a detailed low-temperature thermoluminescence (TSL) study reveals that all TSL peak intensities and trap depths decrease in the Y admixture. The whole phenomenology indicates that a joint effect of "band-gap engineering" and "defect engineering" works in LuYAG:Pr ceramics, as confirmed by the comparison between TSL data, radioluminescence temperature-dependence measurements, and first-principles calculations. As a consequence of material optimization, the light yield of LuYAG:Pr ceramics with 25% Y is found to be 24 400 ph/MeV with a short 1.0-μs shaping time, which is 20% higher than the value obtained for Y-free LuAG:Pr ceramics. We close with an explanation of the role of Y that also suggests future research directions concerning other oxide scintillators.

DOI: 10.1103/PhysRevApplied.6.064026

I. INTRODUCTION

The research on high-light-yield, high-density, and fast scintillators is mainly driven by modern imaging techniques such as positron emission tomography (PET). Garnet scintillators are promising for their high figure of merit. Among them, $Lu_3Al_5O_{12}$: Pr (LuAG:Pr) offers a short decay time (approximately 20 ns) and high light yield (from approximately 16 000 to 19 000 ph/MeV) [1]. Therefore, LuAG:Pr together with $Lu_2Si_2O_5$:Ce (LSO:Ce) are regarded as the most promising candidate scintillators for TOF PET [2]. Additionally, PEM (positron emission mammography) for breast cancer detection has already been developed by using a LuAG:Pr single-crystal pixelated array [3]. However, shallow traps due to intrinsic defects have always been a serious drawback in these garnet materials. During the tens or even hundreds of nanometers of free-carrier migration [4,5] during the transport stage of the scintillation process, carrier trapping in shallow defects causes slow scintillation tails. As a result, a slow component of 476 ns in scintillation decay is observed in LuAG:Pr single crystals [6]. Moreover, intrinsic defect variants, similar to shallow traps, cause ultraviolet (UV) host luminescence. Low-temperature radioluminescence (RL) spectra of LuAG:Pr single crystals illustrate that the host luminescence emission has an intensity comparable to that of Pr^{3+} $5d$-$4f$ transitions [6]. Systematic studies [7–11] were performed to investigate the relationship between the host luminescence and related defects in these garnet materials. Two kinds of host luminescence in undoped LuAG single crystals were evidenced by synchrotron radiation vacuum ultraviolet spectroscopy [7,8,10]: (i) fast (nanosecond) self-trapped exciton emission peaking at 4.96 eV [7] and (ii) slow (microsecond) emission peaking at 4.9 and 3.65 eV, which can be ascribed to the two configurations of an exciton localized at Lu_{Al} antisite defects [10].

The suppression of intrinsic defects, especially Lu_{Al} antisites, is of great importance for achieving LuAG:Pr scintillators with high figures of merit. A $Lu_3(Ga, Al)_5O_{12}$: Pr (LuGAG:Pr) scintillator was proposed [12] that showed no antisite defects. Detailed studies [6] revealed that the host luminescence is suppressed even for a low Ga content. In addition, slow decay processes are also suppressed by Ga^{3+} admixture [6,12]. Such effects are explained by a "band-gap" phenomenon [13,14]. In other words, the conduction band shifts to lower energy so reducing the trapping capability of Lu_{Al} antisite defects [14]. Unfortunately, a simultaneous reduction of the thermal ionization energy of Pr^{3+} $5d_1$ energy levels occurs. As a result, the light yield of LuGAG:Pr is reduced even with 10% Ga admixing [6]. Very recently, a systematic study [13] reveals that "band-gap and band-edge engineering" works not only in LuGAG:Pr but also in various cation ion-(such as In, As, Sb, Gd) admixed LuAG scintillators.

Another way to control defects in oxide scintillators is the "defect-engineering" approach aimed at reducing the defect concentration in the materials. This method is shown to work in various scintillators such as, for example, La-doped $PbWO_4$ [15,16] and Mg-codoped LuAG:Ce [17,18]. Defect concentration is reduced by introducing small

*lijiang@mail.sic.ac.cn
†huaminkou@mail.sic.ac.cn

amounts (from tens to a few hundred parts per million) of aliovalent impurities. Our recent work shows that by Mg codoping, the light yield of LuAG:Ce ceramics can reach 25 000 ph/MeV with weak, slow scintillation tails [18].

In addition, Y admixture has been exploited in place of several oxide scintillators such as $(Lu, Y)_2SiO_5:Ce$ [19] and $(Lu, Y)AlO_3:Ce$ [20]. Several studies of Y admixture in LuAG:Pr single crystals were also performed [21,22]. Very recently, a significant light-yield increase upon a 25% Y admixing was obtained [23]. The relative weight of the fast scintillation-decay component was also simultaneously increased [24]. However, the explanation of this improvement remains uncertain. In addition, the host luminescence still exists in LuYAG:Pr single crystals [25], which demonstrates that further optimization is still needed to eliminate the responsible defects. Thermoluminescence (TSL) studies above room temperature (RT) show that all trap depths decrease proportionally to Y concentration [24]. This suggests that band-gap engineering might work in the Y-admixed garnet scintillators. Moreover, former theoretical calculation studies found that the formation energies of most intrinsic defects—including antisites—are lower in LuAG than in YAG [25,26]. This indicates that defect engineering might also work in LuYAG:Pr scintillators.

Here, we show that the beneficial effect of Y codoping operates not only in garnet single crystals but also in garnet ceramics doped with Pr^{3+}. It consists of the removal of shallow-trap defects accompanied by an improvement of the scintillation performance. An explanation of the role of Y is proposed, which might give hints for the future research concerning various oxide scintillators.

II. EXPERIMENTAL METHODS

LuAG:Pr and LuYAG:Pr ceramics are fabricated by the solid-state reaction method and further subjected to a high-temperature (1450 °C) air-annealing process in order to improve their scintillation performance. The detailed fabrication process is the same as in our previous works [18,27,28]. No sintering aids are used [27]. Commercial Lu_2O_3, Y_2O_3, Al_2O_3, and Pr_6O_{11} (>99.99% purity) powders are weighed according to the formula $(Lu_{0.9975}, Pr_{0.0025})_3Al_5O_{12}$ and $[(Lu_{0.75}, Y_{0.25})_{0.9975}, Pr_{0.0025}]_3Al_5O_{12}$. Round plates with dimensions of $\Phi 14 \times 1$ mm^2 are cut and polished for most of the experiments, and $\Phi 14 \times 2$ mm^2 samples are polished for the pulse height and scintillation-decay measurements.

The temperature-dependent photoluminescence (PL) spectra are collected by a Hitachi F-4600 spectrophotometer with xenon-lamp excitation and 2.5-nm excitation and emission slits. Temperatures from 20 °C to 380 °C are monitored with a homemade temperature controller. The holding time is 3 min for each temperature. The temperature-dependent RL measurements are carried out with an x-ray tube operated at 72.5 kV and 2.5 mA coupled to an Ocean Optics QE65000 spectrometer based on a charge-coupled-device detector. The spectral sensitivity of the detection system as a function of wavelength is corrected with a standard radon lamp. The measurement temperature is controlled by an Oxford Instruments cryostat Optistat DN-V2 with a temperature range from 77 to 500 K. The light yields of both samples are measured via pulse height with a ^{22}Na (511-keV) γ-ray source excitation. The crystal is optically coupled to the window of a Hamamatsu R2059 photomultiplier tube (PMT). A shaping time from 45 to 3000 ns is adopted. The scintillation decay of the samples is performed with the same setup as the pulse height measurement. The data are acquired by a digital storage oscilloscope (DSO) Agilent 9254. For the TSL study, the ceramics are irradiated at 77 K with the same x-ray tube that is operated at 70 kV and 2.5 mA for 20 min. The samples are glued with silver paint to a copper sample holder. A 0.1-K/s heating rate is adopted. The wavelength-resolved TSL measurements are collected with the same spectrometer used for the RL measurements. The glow curves related to the Pr^{3+} $5d$-$4f$ and $4f$-$4f$ emission transitions are obtained after integration of wavelength-resolved data from 270 to 450 nm and from 450 to 700 nm, respectively.

The first-principles calculations on LuAG and YAG are performed with the Vienna *ab initio* simulation package code [29] with a projector-augmented-wave method [30,31] and a supercell model consisting of 160 atoms. The Perdew-Burke-Ernzerhof (PBE) [32] generalized-gradient approximation is used as the exchange and correlation functionals. The plane convergence is tested with wave basis sets and energy cutoff (550 eV) and k-point sampling ($2 \times 2 \times 2$ k-point meshes of the Monkhorst-Pack type [33]). The Lu $4f$, $5s$, $5p$, $5d$, $6s$, Y $4s$, $4p$, $4d$, $5s$, Al $3s$, $3p$, and O $2s$, $2p$ electrons are described as valence electrons. All geometry optimizations are performed via a conjugate-gradient method with a force tolerance of 0.01 eV/Å.

III. RESULTS AND DISCUSSION

A. Y-induced removal of host luminescence

The x-ray RL spectra of LuAG:Pr and LuYAG:Pr measured at RT and 77 K are displayed in Fig. 1(a). According to different radiative levels of Pr^{3+}, the spectra can be divided into two parts: (i) from 270 to 450 nm and (ii) from 450 to 900 nm, due to the $5d$-$4f$ and $4f$-$4f$ transition of Pr^{3+}, respectively. Compared to LuAG:Pr, the intensity of the sharp emissions due to the $4f$-$4f$ transitions is much higher in LuYAG:Pr than that in LuAG:Pr. This is ascribed to a higher efficiency of the thermally driven transition from the relaxed $5d_1$ to the ^3P_x and $^1D_2$ $4f$ states [34,35]. On the other hand, the intensity of the broad emission band due to the $5d$-$4f$ transition in LuYAG:Pr is almost the same as in LuAG:Pr.

Additional emissions from 200 to 270 nm are found in the RL spectrum of LuAG:Pr. As mentioned in the Introduction,

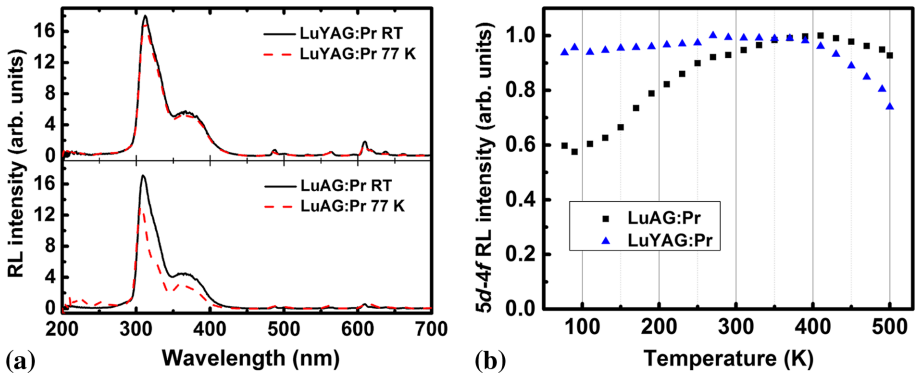

FIG. 1. (a) RL spectra of LuAG:Pr and LuYAG:Pr at RT (291 K) and at 77 K; (b) temperature dependence of the $5d$-$4f$ transition intensity of Pr^{3+} in LuAG:Pr and LuYAG:Pr.

they are related to intrinsic defects of the host matrix. For LuAG:Pr and LuAG:Ce single crystals [36,37], the problem of host luminescence due to antisite defects is serious because of their high melting temperature. In these single-crystal counterparts, the host luminescence intensity can be comparable to Ce^{3+} and Pr^{3+} $5d$-$4f$ transition intensity at 80 K [36,37]. The host luminescence totally disappears in LuYAG:Pr ceramics even at 77 K. The host luminescence suppression in garnet single crystals is found only in Ga^{3+}-admixed LuAG:Pr [12], in which antisite defects are disabled by burying their energy levels into the bottom of the conduction band (CB). The absence of host luminescence in LuYAG:Pr ceramics is caused by a different mechanism. It can be explained *via* two reasons: (i) the relatively low sintering temperature during ceramic preparation that reduces structural defects such as antisites [38] and (ii) the suppression of defects *via* the Y admixture, as we discuss below.

Figure 1(b) shows a complete picture of the RL intensity dependence in both samples. Strong differences are observed below RT, where a clear decrease at low temperature is detected only in LuAG:Pr. Such an effect is due to the carrier trapping at shallow traps that are suppressed by the Y admixture, as we show below. In addition, the drop observed in both cases above RT is caused by the thermal luminescence quenching of Pr^{3+} $5d$-$4f$ emission.

B. Y-induced low-T shift of luminescence quenching

To understand the thermal quenching phenomena, photoluminescence (PL) and photoluminescence-excitation (PLE) spectra of LuAG:Pr and LuYAG:Pr at RT and the temperature dependence of PL and PLE intensities above RT are presented in Figs. 2 and 3. Figure 2 shows that the excitation and emission bands all belong to the fast $5d$-$4f$ transition of Pr^{3+}. In LuAG:Pr ceramics, two excitation bands peaking at 240 and 275 nm and belonging to the transitions of $^3H_4$-$5d_2$ and $^3H_4$-$5d_1$ of Pr^{3+} are seen and agree with previous results [12]. The emission band at 308 and 365 nm in the PL spectrum of LuAG:Pr can be ascribed to the overlapping transition bands from the $5d_1$ state to the $^3H_4$, $^3H_5$, $^3H_6$, and $^3F_{3(4)}$ $4f$ states [34]. This description is also suitable for LuYAG:Pr with only a slight redshift.

The normalized temperature-dependent PL and PLE intensities for LuAG:Pr and LuYAG:Pr are illustrated in Fig. 3. The excitation wavelengths of 240 and 277 nm, and emission wavelength of 310 nm are chosen. The temperature dependence is almost the same for the PL and PLE intensities with various excitation and emission wavelengths whether in LuAG:Pr or LuYAG:Pr ceramics. This suggests that these PL and PLE intensities are all related to the transition of the Pr^{3+} $4f$ levels to the $5d_1$ level because an electron excited to the $5d_2$ level will rapidly relax to the $5d_1$ level. The onset temperature (95% of the peak intensity) of the PL and PLE intensities' decrease is about 420 K for LuAG:Pr and 340 K for LuYAG:Pr ceramics, respectively. In an earlier study, the onset temperature of LuAG:Pr nanopowder is reported to be 450 K [39]. The variation of the values can be ascribed to different Pr^{3+}-doping concentrations in ceramics (0.25 at. %) and

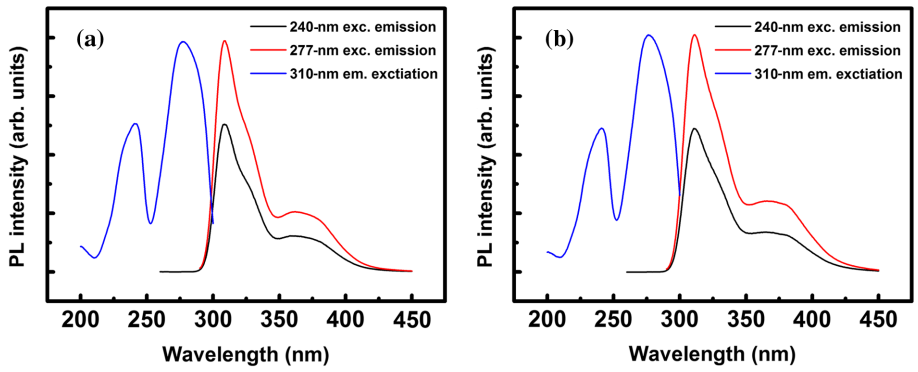

FIG. 2. PL and PLE spectra of LuAG:Pr (a) and LuYAG:Pr (b) at RT (18 °C); excitation and emission wavelengths of 240, 277, and 310 nm are displayed with different line colors.

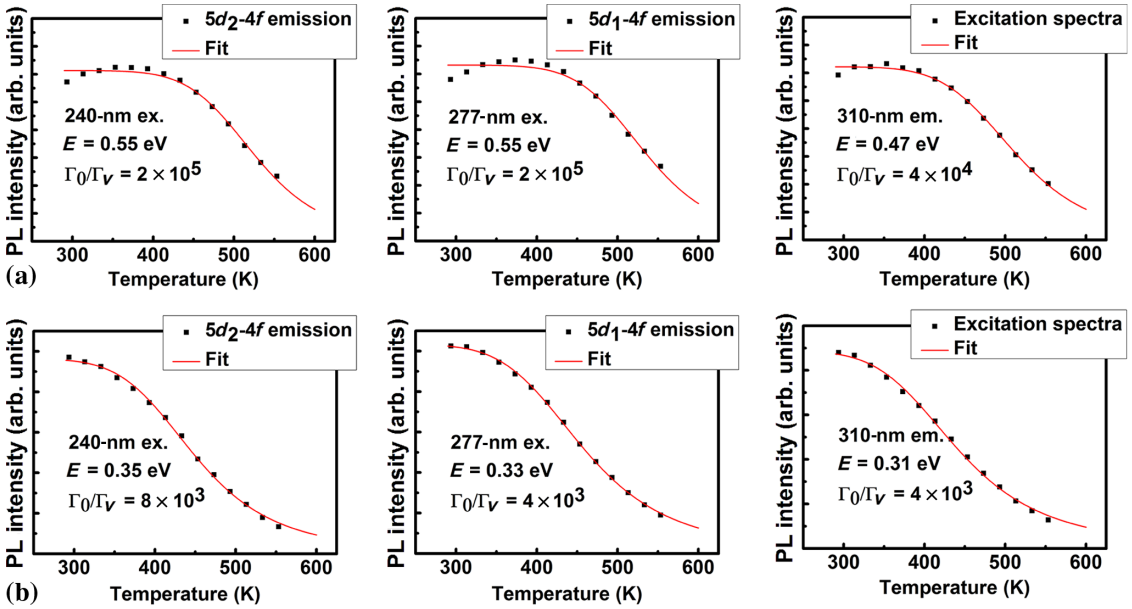

FIG. 3. Temperature-dependent PL and PLE intensities for LuAG:Pr (a) and LuYAG:Pr (b). Excitation wavelengths of 240 and 277 nm, and emission at 310 nm are selected. Solid lines are numerical fits of the data using Eq. (1).

powders (0.1 at. %). This alters the onset temperature due to concentration quenching [40].

Although only 25-at. % Y^{3+} replaced the Lu^{3+} sites, the shift of the onset temperature for LuYAG:Pr is about 80 K. To understand this, it is necessary to study the mechanism of thermal quenching in these ceramics. In general, two processes of thermal quenching are considered in garnet materials [41]: (i) thermal relaxation from the excited state ($5d$ levels) to the ground state ($4f$ levels) through the crossing point [42] and (ii) thermal ionization from the excited state to the bottom of the CB [43]. The main difference between these two processes is whether thermally activated electrons are found in the CB. We assume that the thermal ionization process is dominant in LuAG:Pr and LuYAG:Pr based on the following reasons: (i) there is only a slight difference between Stokes's shift of both samples, indicating similar thermal relaxation processes and (ii) the bottom of the CB is lower in LuYAG:Pr than that of LuAG:Pr. This changes the thermal ionization activation energy. Other measurements such as photocurrent-excitation spectra [41,44] or temperature-dependent UV irradiation TSL [45,46] also confirm our assumption.

We can still use the single-barrier quenching model [Eq. (1)] to describe the thermal quenching process:

$$I(T) = \frac{I_0}{1 + \Gamma_0/\Gamma_v \exp(-E/kT)}, \qquad (1)$$

where I is the PL and PLE intensities, I_0 is the PL and PLE intensities at $T = 0$, Γ_0 and Γ_v are the attempt rate of the nonradiative process and the radiative rate, respectively, E is the activation energy, k is the Boltzmann constant, and T is the temperature. All results on the temperature dependence of the PL and PLE intensities in LuAG:Pr and LuYAG:Pr can be fit to such a model. The parameters are listed in Table I with other data from the PL and PLE spectra. Compared with LuAG:Pr, the activation energy decreases by about 0.2 eV in LuYAG:Pr, decreasing the thermal quenching temperature.

C. Light-yield improvement and slow component suppression

To demonstrate the effect of the Y admixture on scintillation performance, pulse-height measurements under a ^{22}Na γ-ray-source excitation at different time gates are made with both LuAG:Pr and LuYAG:Pr samples. The uncertainties of the light-yield results are within 3%. As illustrated in Fig. 4(a), the light yields of both LuYAG:Pr and LuAG:Pr exceed 2500 p.e./MeV at 1-μs shaping time. By considering the emission-weighted quantum efficiency of the R2059 PMT for both Pr^{3+} doping samples as 13.6%, the light yields of LuAG:Pr and LuYAG:Pr ceramics are estimated to be 20 400 and 24 400 ph/MeV (1-μs shaping time), respectively. The 3-μs light yield of LuYAG:Pr reaches 27400 ph/MeV. This result also shows that Y admixture in LuAG:Pr ceramics can significantly improve the light yield. In order to clarify the reason for this improvement, the scintillation decay of two samples is also measured under a ^{22}Na γ-ray-source excitation and DSO readout. We perform double-exponential approximations to fit both the light-yield and scintillation-decay results. Taking into account the different experimental techniques employed and the uncertainties in

TABLE I. Selected PL and PLE spectra results and parameters of the fit to the temperature-dependent PL and PLE intensities according to Eq. (1).

	Excitation peak Wavelengths (nm)	Emission peak Wavelength (nm)	$5d_1$-$4f$ emission			$5d_2$-$4f$ emission			Excitation		
			E (eV)	Γ_0/Γ_v	Onset (K)	E (eV)	Γ_0/Γ_v	Onset (K)	E (eV)	Γ_0/Γ_v	Onset (K)
LuAG:Pr	240, 275	308	0.55	2×10^5	~420	0.55	2×10^5	~420	0.47	4×10^4	~420
LuYAG:Pr	240, 275	312	0.33	4×10^3	~340	0.35	8×10^3	~340	0.31	4×10^3	~340

both measurements, the fit results obtained from both time-gate-dependent light yield and scintillation-decay curves are consistent. From these results, we conclude that both the decay time and relative intensity of the (1–2)-μs slow component in LuAG:Pr are reduced significantly after Y admixture. Systematic investigations [6,36,47] reveal that the origin of the slow scintillation light is ascribed to the presence of shallow-trap defects—especially antisite defects. Therefore, the suppression of defects by Y admixture decreases the slow components and improves the light yield.

The collection of data obtained from the light-yield and scintillation-decay measurements shown in Fig. 4 is reported also in Table II. As we note above, even though they are very different kinds of measurements, both the gate-dependent light yield and scintillation data give compatible results. After Y admixture, the relative intensity of the fast component reaches more than 60%, a higher percentage than LuYAG:Pr single crystals [24]. The 200-ns light yield of LuYAG:Pr reaches 71% of the 3-μs light yield, 6% higher than LuAG:Pr. The ratio between the 1- and 3-μs light yield of LuYAG:Pr is 10% higher than in LuAG:Pr. These results confirm that Y admixture in LuAG:Pr improves the light yield by reducing the defect-related slow component in the LuAG host.

D. Low-temperature TSL study

The results of the light yield and low-temperature RL indicate that shallow electron traps such as antisite defects are suppressed by this Y-admixture strategy. In this section of the article, we explain these results by characterizing all shallow electron traps in LuYAG:Pr and LuAG:Pr using low-temperature TSL.

Figure 5 shows the contour plot of wavelength-resolved TSL measurements performed on both LuAG:Pr and LuYAG:Pr. The emission spectra of both samples consist of two parts: (i) the emission range from 270 to 450 nm due to the $5d$-$4f$ transition of Pr^{3+} and (ii) the emission range above 450 nm due to the $4f$-$4f$ transition of Pr^{3+}. We plot TSL glow curves from the $5d$-$4f$ and $4f$-$4f$ transitions by integrating the glow intensities from 270 to 450 nm and 450 to 700 nm, respectively. We find that the shapes and peak temperatures of both curves are about the same with the

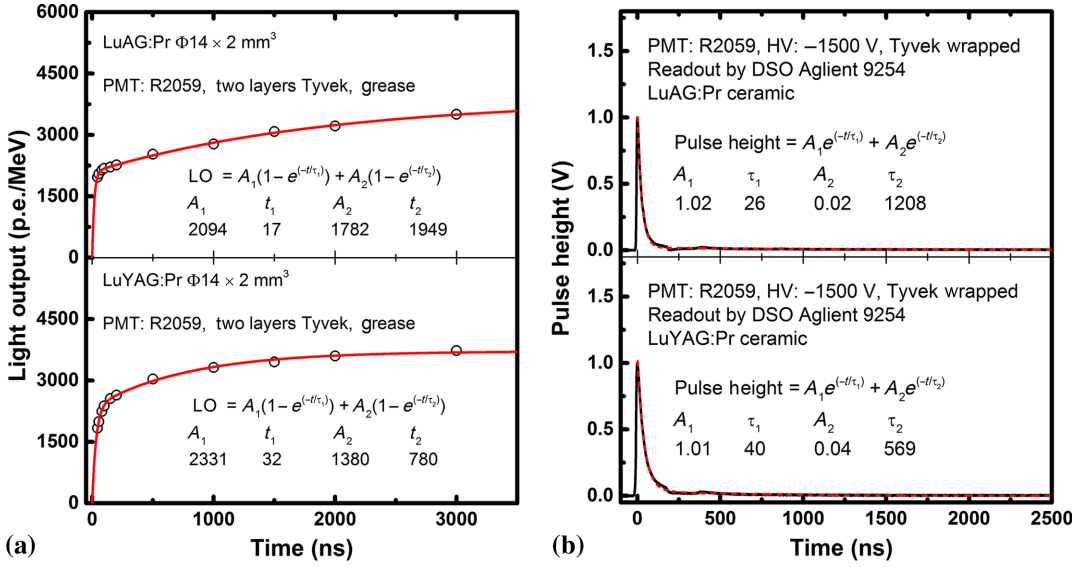

FIG. 4. (a) Light yield of Φ14 × 2 mm LuAG: Pr and LuYAG:Pr ceramics measured at various time gates (excitation with 511-keV photons from a 22-Na source) from 45 to 3000 ns. A double-exponential function $\mathrm{LO} = \sum_{i=1,2} A_i \exp(1 - e^{(-t/\tau_i)})$ is used to fit the time-gate dependence. The relative intensities of each component $I_i = A_i/\sum_{j=1,2} A_j \times 100$ ($i = 1, 2$) are also calculated. (b) Normalized scintillation-decay curves monitored by DSO (excitation ^{22}Na 511 keV) of both ceramics. A double-exponential function $I = \sum_{i=1,2} A_i \exp(-t/\tau_i)$ is used to fit the scintillation-decay curves (red line). The relative intensities of each component $I_i = A_i\tau_i/\sum_{j=1,2} A_j\tau_j \times 100$ ($i = 1, 2$) are also reported.

TABLE II. Light yields (LY) of $\Phi 14 \times 2$ mm LuAG: Pr and LuYAG:Pr ceramics at 200-, 1000-, and 3000-ns time gates are reported together with their relative ratios. Decay-time components and their relative intensities obtained from time-gate-dependent light yield and scintillation decay are also reported.

				Fit results from light yield		Fit results from scintillation decay			
	200 ns (ph/MeV)	1000 ns (ph/MeV)	3000 ns (ph/MeV)	τ_1(ns)/ I_1(%)	τ_2(ns)/ I_2(%)	τ_1(ns)/ I_1(%)	τ_2(ns)/ I_2(%)	LY(200)/ LY(3000)	LY(1000)/ LY(3000)
LuAG:Pr	16 700	20 400	25 800	17/54	1949/46	26/52	1208/48	65%	79%
LuYAG:Pr	19 400	24 400	27 400	32/63	780/37	40/64	569/36	71%	89%

only differences in peak intensity due to different intensities of the $5d$-$4f$ and $4f$-$4f$ transitions. The TSL glow curves related to the $5d$-$4f$ transition are chosen to study shallow electron traps in both LuAG:Pr and LuYAG:Pr due to their higher signal-to-noise ratio.

Figure 6(a) reports the glow curves of both the LuAG:Pr and LuYAG:Pr samples obtained after integration over that range. The shape and maximum position of the TSL glow peaks are slightly modified by the correction performed for the thermal quenching of luminescence using the parameters from fits of temperature-dependent PL intensities [46]. The corrected glow curves are shown in Fig. 6(b). Five sharp glow peaks marked from *A* to *E* are found in LuAG:Pr, while six peaks marked from *A*' to *E*' and *F* are found in LuYAG:Pr. These notations show the one-to-one correspondence of these peaks (except for *F*) in both samples. Compared with LuAG:Pr, two significant modifications occur in LuYAG:Pr: (i) all TSL peak intensities decrease and (ii) all TSL peaks shift to lower temperatures. The intensity decrease confirms the reduction of shallow-trap-defect concentrations in LuYAG:Pr. The typical peak for antisite defects [36] (around 150 K) coincides with peak *A* and/or *B* in the LuAG:Pr TSL glow curve. Their intensities also decrease in LuYAG:Pr, suggesting a reduction of intrinsic defects in agreement with the absence of host luminescence in such ceramic. In addition, the temperature shift suggests that band-gap engineering may work in LuYAG:Pr samples.

A deeper investigation of the TSL glow curves of both samples is performed by the "partial cleaning and initial rise method," as performed in numerous previous studies on other oxide scintillators [47–49]. X-ray irradiation of the samples at 77 K is followed by heating to a partial cleaning temperature T_{stop} and by a rapid cooling to 77 K; finally, the glow curve is recorded with a heating rate of 0.1 K/s. A simple exponential function is then used to fit the initial portion of each peak:

$$I(T) = I_0 \exp(-E_T/kT), \tag{2}$$

where $I(T)$ is the TSL intensities, E_T is the trap depth, and k is the Boltzmann constant (Fig. 7). The different T_{stop} temperatures chosen for each peak in Fig. 6(b) are shown in Table III. The trap-depth values of LuAG:Pr and LuYAG:Pr are calculated by using Eq. (2). Once the trap depth is calculated, the frequency factor s is also evaluated according to [50]

$$s = (\beta E_T/kT_m^2)\exp[E_T/kT_m]. \tag{3}$$

Hence, the detrapping time τ at a given temperature T can be calculated as

$$\tau = s^{-1}\exp(E_T/kT). \tag{4}$$

Here, E_T (eV) is the trap depth of the peak, k is the Boltzmann constant, and β (K/s) is the heating rate. The

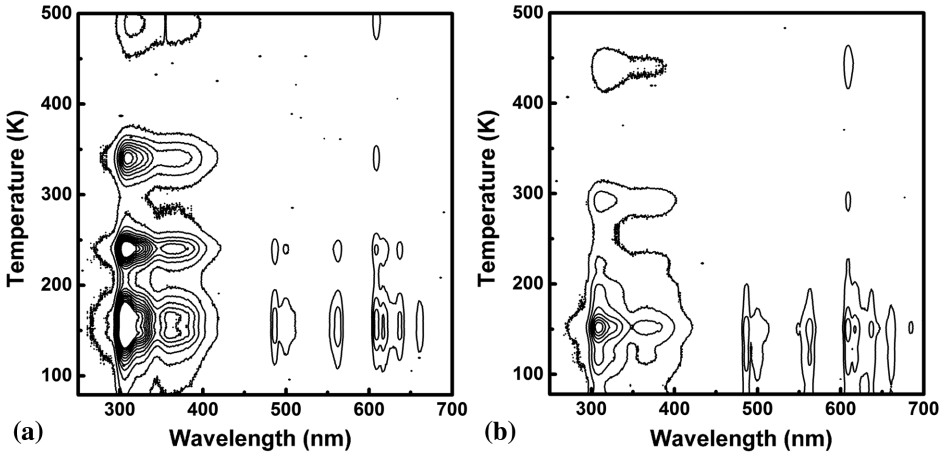

FIG. 5. Contour plot of wavelength-resolved TSL measurements performed on (a) LuAG:Pr and (b) LuYAG:Pr after x-ray irradiation at 77 K. Heating rate = 0.1 K/s.

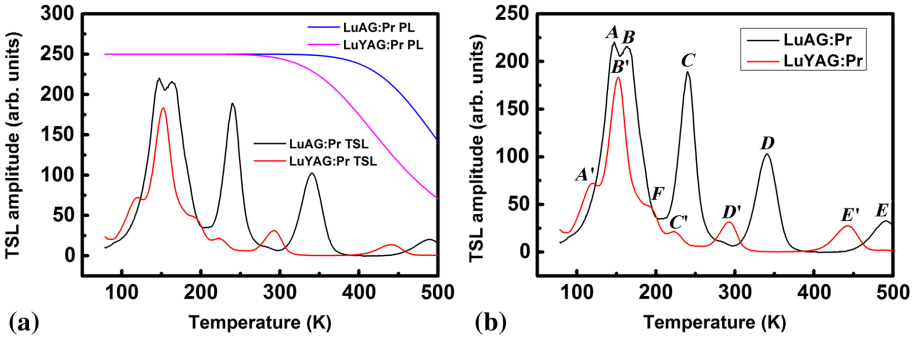

FIG. 6. TSL glow curves for LuAG:Pr and LuYAG:Pr integrated in the $5d$-$4f$ emission range (a) as measured and (b) corrected for the PL intensity temperature dependences reported as blue and pink lines in panel (a).

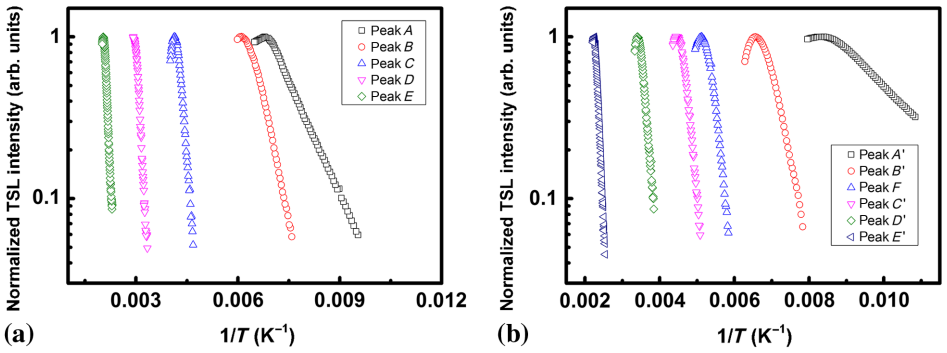

FIG. 7. Arrhenius plots of the TSL of (a) LuAG:Pr and (b) LuYAG:Pr following x-ray irradiation at 77 K and partial cleaning at different T_{stop} temperatures. The curves are corrected for the thermal quenching of Pr^{3+} emission and normalized to their maximum.

trap depth, frequency factor, and detrapping time at RT (298 K) are reported in Table III for all the investigated TSL peaks in both samples. The errors for the trap depth are within 10%, while the errors for the frequency factors calculated from Eq. (3) have a larger uncertainty. Thus, we can rely only on their order of magnitude. This is also the case for mean detrapping times.

Some comments are deserved for the correlation between the decay times of the scintillation slow components and the lifetimes of the traps. Although, in principle, they should have the same values, such a direct correspondence is rarely observed in practice. Additional slow components added to fit the queue of the scintillation decay are much dependent also on the time window of the measurement that is limited to the microsecond time scale in our case. In other words, in our case, the slow components and lifetimes of the TSL peaks should be considered as complementary sources of information on the scintillation mechanism rather than two manifestations of exactly the same defects.

From our overall results—namely, the scintillation slow-decay components and TSL—it appears that Y codoping has the capability to reduce the concentration and thermal

TABLE III. Parameters of TSL glow-curve peaks in LuAG:Pr and LuYAG:Pr evaluated by the partial cleaning and initial rise method. The errors for trap-depth values are also reported in parentheses.

TSL peak temperature (K)	T_{stop} (K)	Trap depth (eV)	Frequency factor (s^{-1})	Detrapping time at RT (s)
		LuAG: Pr		
147 (A)	131	0.09 (7.6%)	$\sim 10^{1}$	$\sim 10^{1}$
163 (B)	151	0.20 (5.5%)	$\sim 10^{4}$	$\sim 10^{-1}$
240 (C)	229	0.55 (7.3%)	$\sim 10^{9}$	$\sim 10^{0}$
340 (D)	323	0.75,(5.3%)	$\sim 10^{9}$	$\sim 10^{4}$
490 (E)	466	0.99 (8.1%)	$\sim 10^{8}$	$\sim 10^{9}$
		LuYAG: Pr		
121 (A')	107	0.05 (7.4%)	$\sim 10^{0}$	$\sim 10^{1}$
152 (B')	138	0.16 (6.1%)	$\sim 10^{3}$	$\sim 10^{1}$
190 (C')	179	0.41 (4.9%)	$\sim 10^{9}$	$\sim 10^{-2}$
223 (D')	210	0.47 (8.5%)	$\sim 10^{9}$	$\sim 10^{-1}$
292 (E')	279	0.62 (9.7%)	$\sim 10^{8}$	$\sim 10^{2}$
442 (F')	416	0.92 (4.3%)	$\sim 10^{8}$	$\sim 10^{7}$

stability of a wide variety of defects with very different lifetimes, from microseconds to seconds and even longer. These defects include antisite defects together possibly with other defects with different structure, although probably with a common general intrinsic nature. In Table II, the improvement is evidenced for a reduction of traps with a decay time in the microsecond time scale (the slow-decay component is observed to become weaker). TSL reveals a positive effect of Y also for deeper levels. We cannot exclude the presence of other TSL peaks at temperatures below 100 K, outside our investigation range, due to traps possessing lifetimes in the microsecond time scale.

Antisites are usually referred to as correlated to peaks in the 150-K range, whose lifetimes here observed for ceramics are higher (0.1–1 s) with respect to those observed for single crystals (10^{-4} s; see Refs. [36,47]). Although this result appears strange, it might be explained by the dependence of the detrapping process on the local structure of defects, which might be very different for single crystals and for ceramics. Such a phenomenology certainly deserves deeper investigations involving TSL and other parallel studies, for example, electron paramagnetic resonance, to investigate the structure of TSL active defects in ceramics and in single crystals.

E. Defect engineering in LuYAG:Pr

Defect engineering, as the name says, is a defect-control methodology by reducing the defect concentration through codoping or composition tuning in scintillators. The comparison between the TSL intensity of LuAG:Pr and LuYAG:Pr ceramics already shows that defect engineering works in the Y admixture. This is in accordance with the previous first-principles calculation results reporting that, compared with LuAG, defect concentrations of all intrinsic defects, including antisite defects, are lower in YAG due to its higher defect-formation energy [25,26]. An application of this mechanism in LuYAG:Pr is found when we relate the TSL results with temperature-dependent host luminescence and Pr^{3+} $5d$-$4f$ RL intensities. Figure 8(a) shows a comparison of the temperature-dependent host luminescence intensity and TSL in LuAG:Pr. As can be seen from the picture, the host luminescence intensity decreases sharply from 100 to 200 K, in accordance with previous VUV experiments on LuAG single crystals [10] and due to thermal quenching. We use the single-barrier quenching model [Eq. (1)] to fit the temperature dependence of such intensity. The calculated activation energy of the host luminescence thermal quenching is 0.10 eV, which is close to the trap depth of peak *A* (0.09 eV). We, thus, suggest that quenching of host luminescence induced by antisite defects in LuAG is related to peak *A* in the TSL glow curve.

Another demonstration that defect engineering operates with Y admixture is revealed by combining the temperature-dependent RL and TSL results. The increasing part in the temperature-dependent RL intensities of LuAG:Pr in Fig. 1(b) can be explained by releasing of shallow traps [51–53]. At low temperature, shallow traps can be considered as nonradiative centers because the mean detrapping time calculated by Eq. (4) is very long. After heating to a certain temperature, some of the shallow traps do not trap carriers in a stable way anymore and do not compete with the Pr^{3+} $5d$-$4f$ emission centers anymore. Therefore, RL intensity increases as the temperature increases. To confirm this explanation, we integrate the TSL intensity of LuAG:Pr over the temperature and superimpose it to the temperature-dependent RL intensities in Fig. 8(b). The two curves are similar in the temperature range of 77 to 410 K. This confirms that our assumptions on defect release are correct. Poor correlation is observed only beyond 410 K due to thermal quenching of the Pr^{3+} $5d$-$4f$ transition. Therefore, except for deriving host luminescence, the shallow-trap defects in LuAG:Pr ceramics can also act as stable nonradiative centers at low temperatures that deteriorate the steady-state scintillation efficiency by competing with Pr^{3+} emission centers in free-carrier capture. Compared with LuAG:Pr, the RL intensities of LuYAG:Pr are rather stable from 77 to 400 K [Fig. 1(b)], in accordance with the lower concentration and lower thermal stability of traps occurring in LuYAG:Pr.

F. Band-gap engineering in LuYAG:Pr

In addition to defect engineering, band-gap engineering also works in Y-admixed LuAG:Pr. As shown in the TSL study, the TSL peaks shift to lower temperature in LuYAG:Pr. Figure 9 illustrates the correspondence

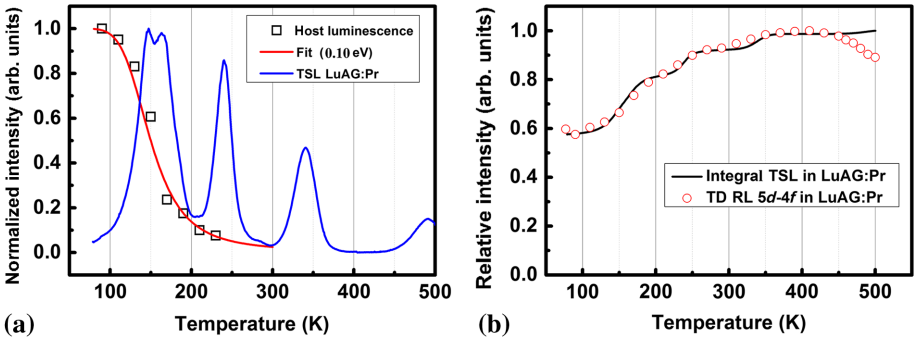

FIG. 8. (a) Comparison between the temperature dependence of the host luminescence and the TSL glow curve of LuAG:Pr. Red line is the fit of the temperature dependence of the host luminescence intensities by using the single-barrier quenching model. (b) Correlation between the temperature dependence of the Pr^{3+} $5d$-$4f$ transition and TSL integral (calculated by integrating the TSL glow curve up to the temperature specified in the *x* axis) of LuAG:Pr.

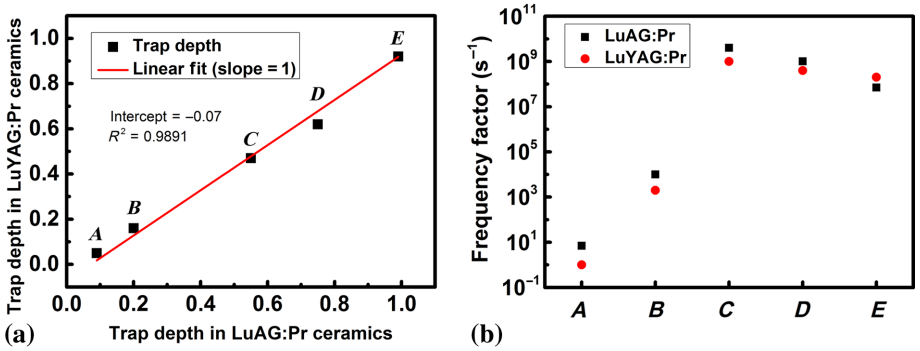

FIG. 9. Correspondence between the (a) trap depth and (b) frequency factor of all related peaks in LuAG:Pr and LuYAG:Pr calculated by analyzing TSL data obtained from the partial cleaning and initial rise method.

between the calculated trap depths and frequency factors of each peak from *A* to *E* in LuAG:Pr and *A*' to *E*' in LuYAG:Pr. By using a linear fit with slope 1, we find that all trap depths in LuYAG:Pr are about 0.07 eV less than that in LuAG:Pr. On the other hand, these defects' frequency factors remain the same order of magnitude for the two samples. Therefore, the shift of the peak temperature in LuYAG:Pr can be ascribed to the trap depth decrease rather than the frequency factor modification, unlike what is observed in other cases [49,54]. As all trap depths shrink in LuYAG:Pr, we speculate that the shift in the trap depth is induced by a shift of the CB bottom.

To shed light on the electronic structure and defect concentration change in LuYAG:Pr, first-principles calculations on both LuAG and YAG are performed. Here, we are interested in the modification of the band gap and defect-formation energy between these two materials. Table IV shows the calculated lattice constant, band gap, and antisite defect-formation energy in both YAG and LuAG.

Some of the results on LuAG are taken from our previous works [38]. The deviation of the calculated lattice constant from the experimental results is within 1%. Although the band gap is underestimated due to density-functional theory (DFT), the change in band gaps between the two materials, which is the most important point in this work, agrees with experimental results. Compared to LuAG, the calculated band gap of YAG shrinks by 0.29 eV, which is in accordance with the experimental results (0.3 eV). The change of band gap between LuYAG:Pr (with 25% Y) and LuAG:Pr also agrees with our calculation results if we assume that the shrinkage between LuYAG:Pr and LuAG:Pr is proportional to the Y content in LuYAG:Pr [24], as indicated in the LuYAG:Pr single crystals. In addition, the antisite defect-formation energy is higher in YAG, which explains the absence of antisite defect-induced host luminescence in the LuYAG:Pr sample. The calculated band structures of LuAG and YAG are shown in Fig. 10.

Finally, through a combination of TSL and DFT studies, we conclude that band-gap engineering works in the LuYAG:Pr sample with a 0.07-eV shift of trap levels by a 25% Y admixture. The shallow electron traps with trap depth lower than 0.07 eV in LuAG:Pr are then all buried in the conduction band. On the other hand, this modification of the band structure also reduces the ionization energy of the Pr^{3+} $5d_1$ level [60], which finally causes luminescence quenching. This phenomenon is evident in Ga-admixed LuAG:Pr single crystals [6]. With only 10% Ga^{3+} replacement on the Al^{3+} site in LuAG, the light yield drops about

TABLE IV. Calculated lattice constant (a), antisite-defect-formation energy [E^f(AD)], and band gap (E_g) of LuAG and YAG using the PBE functional.

	a(Å)	E^f(AD)[a] (eV)	E_g (eV)
		YAG	
This work	12.112	0.979 eV	4.49 eV
Ref.	12.114[b]	1.232 eV[c]	4.71 eV[d]
Expt.	12.000[e]	⋯	7.5 eV[f]
		LuAG	
This work	12.021	0.822 eV	4.78 eV
Expt.	11.906[e]	⋯	7.8 eV[f]

[a]Formation energy of the dominant antisite defect, that is, $Lu_{Al,16a}$ (or $Y_{Al,16a}$) occurring under Lu_2O_3 (or Y_2O_3) excess condition. See Ref. [38] for more details.
[b]Derived from Ref. [55].
[c]Derived from Ref. [56].
[d]Derived from Ref. [57].
[e]Derived from Ref. [58].
[f]Derived from Ref. [59].

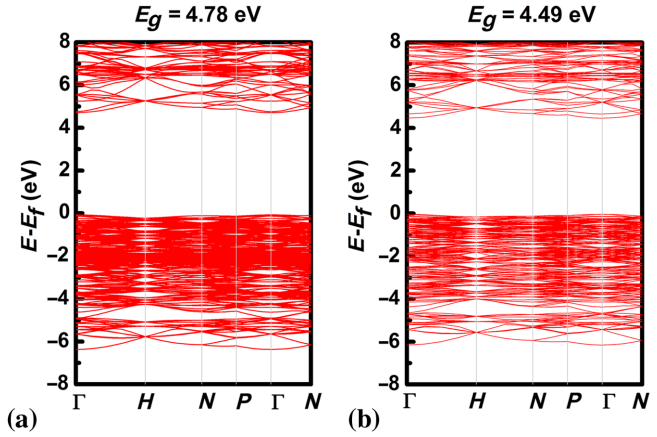

FIG. 10. Calculated band structure of (a) LuAG and (b) YAG along high-symmetry lines.

15%–20% [6]. Our thermal ionization data indicate that the values of the luminescence-quenching onset temperature and the activation energy of temperature-dependent PL intensities are both lower in LuYAG:Pr than that in LuAG:Pr. Fortunately, the onset temperature of 25% Y-admixed LuAG:Pr is 340 K, still well above RT. A further Y concentration increase can certainly decrease the onset temperature below RT, thus, deteriorating its RT steady-state scintillation efficiency and light yield. Previous investigations of LuYAG:Pr single crystals [23,24] compared the light yield of 25% Y-admixing samples with 50% and 75% Y-admixed LuAG:Pr—these dropped by 19% and 24%, respectively. Therefore, 25% seems to be the optimal Y content in LuYAG:Pr.

G. Applicability of the Y-admixture strategy

In the past, band-gap engineering and defect engineering were regarded as two separate ways to improve scintillation performance. In this article, we determine that these two strategies can be effective in one material system. The success of the LuYAG:Pr scintillator will pave a way to defect control in scintillators.

In addition, Y-admixed LuAG:Pr is another successful example of the rare-earth cation-admixture approach in wide-band-gap scintillators. This strategy has already been adopted in almost all important oxide scintillators, not only by Y^{3+} replacement on Lu^{3+} sites such as LYSO:Ce [19], LuYAP:Ce [20], LuYAG:Ce [22] but also by other admixture approaches, such as La-admixed GPS:Ce [61], Gd-admixed LSO:Ce [54], Gd-admixed LuGAG:Ce [62], and Sc-admixed $LuBO_3$:Ce [63]. Although differences exist in these cases, one important mechanism should be taken into consideration, that is the balance between band-structure design and defect-concentration control. Unlike LuYAG:Pr, for most of the above scintillators, one of these two aspects may be dominant. In most of the garnet, perovskite, and silicate scintillators, such as LuYAG:Ce, LuYAP:Ce, LYSO:Ce, and LGSO:Ce, where the defects play an important role, the admixture of the rare-earth cation with a large ionic radius reduces the defect concentration and improves scintillation performance. This has already been proved by first-principles calculations [25,26] and themoluminescence [54]. On the other hand, the effect of band-gap engineering [13] should not been neglected, especially in scintillators such as LuYAG:Pr, GLuGAG:Ce, LaGPS:Ce, and LuScBO3:Ce, where a bigger cation admixture always shrinks the band gap, decreases the bottom of the CB, and influences the shallow trap and thermal ionization energy [60,63]. Therefore, a deep investigation of the defects and band structure of these mixed scintillators should be performed for their further scintillation performance optimization.

Finally, we present an energy-level scheme (Fig. 11) in LuAG:Pr and LuYAG:Pr to visualize the role of Y admixture.

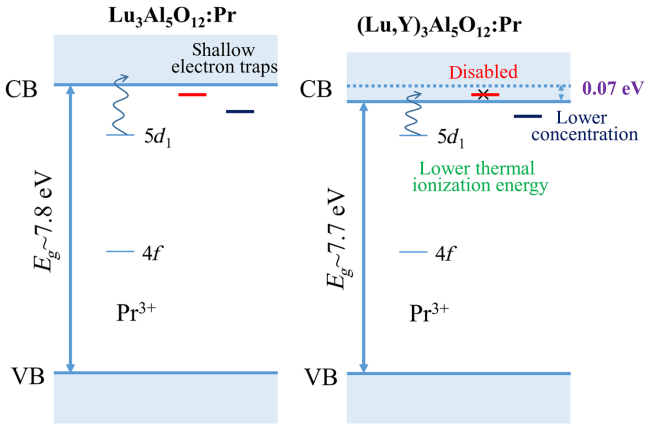

FIG. 11. Comparison of the energy-level scheme in LuAG:Pr and LuYAG:Pr.

IV. CONCLUSIONS

Host luminescence and thermoluminescence glow peaks are evidence of intrinsic defects in LuAG:Pr. Here, we propose a host-luminescence-free LuAG:Pr ceramic scintillator by Y admixture. The role of Y in LuYAG:Pr is studied. The lower position of the Y $4p$ energy level causes a shift in the conduction-band bottom of the LuAG:Pr. As a consequence, the edge of the conduction band decreases to 0.07 eV by 25% Y admixing in LuAG:Pr, as demonstrated by TSL measurements. Moreover, the Y admixture decreases the concentration of intrinsic defects due to their higher formation energy in YAG with respect to LuAG [25,26]. Therefore, fewer shallow-trap defects are found in the Y-admixed samples. This also explains the disappearance of host luminescence. Hence, the scintillation performance of LuYAG:Pr is controlled by the above two factors; 25% Y turns out to be the optimal concentration in LuYAG:Pr due to a balance between the defect suppression and the thermal ionization energy decrease.

Finally, the LuYAG:Pr ceramic with 25% Y features a light yield as high as 24 400 and 27 400 ph/MeV (1.0- and 3.0-μs shaping time, respectively) and a fast scintillation-decay component with a relative intensity of 63%. Recalling also the high density of the material (6.2 g/cm^3), it is possible to conclude that the LuYAG:Pr ceramic is a promising scintillator candidate for both high-energy physics and medical-imaging applications. The absence of antisite defects inducing host luminescence proves that high-performance scintillators with few defects can be achieved by a ceramic fabrication process. Further optimization on the composition and annealing process is still planned to obtain ceramics with possibly higher figures of merit.

ACKNOWLEDGMENTS

This work is supported by the National Natural Science Foundation of China (Grants No. U1332202, 61675221),

and the Science and Technology Commission of Shanghai Municipality (Grant No. 15520721000). A. V. is grateful for the support by the CAS President's International Fellowship Initiative (Grant No. 2014VTB009).

[1] W. Drozdowski, P. Dorenbos, J. T. M. de Haas, R. Drozdowska, A. Owens, K. Kamada, K. Tsutsumi, Y. Usuki, T. Yanagida, and A. Yoshikawa, Scintillation properties of praseodymium activated $Lu_3Al_5O_{12}$ single crystals, IEEE Trans. Nucl. Sci. **55**, 2420 (2008).

[2] M. Conti, L. Eriksson, H. Rothfuss, and C. L. Melcher, Comparison of fast scintillators with TOF PET potential, IEEE Trans. Nucl. Sci. **56**, 926 (2009).

[3] A. Yoshikawa, T. Yanagida, K. Kamada, Y. Yokota, J. Pejchal, A. Yamaji, Y. Usuki, S. Yamamoto, M. Miyake, K. Kumagai, K. Sasaki, T. R. dos Santos, M. Baba, M. Ito, M. Takeda, N. Ohuchi, and M. Nikl, Positron emission mammography using Pr:LuAG scintillator – Fusion of optical material study and systems engineering, Opt. Mater. **32**, 1294 (2010).

[4] R. Kirkin, V. V. Mikhailin, and A. N. Vasil'ev, Recombination of correlated electron-hole pairs with account of hot capture with emission of optical phonons, IEEE Trans. Nucl. Sci. **59**, 2057 (2012).

[5] A. Belsky, K. Ivanovskikh, A. Vasil'ev, M.-F. Joubert, and C. Dujardin, Estimation of the electron thermalization length in ionic materials, J. Phys. Chem. Lett. **4**, 3534 (2013).

[6] H. Ogino, K. Kamada, A. Yoshikawa, F. Saito, J. Pejchal, J. A. Mareš, M. Nikl, A. Vedda, J.-i. Shimoyama, and K. Kishio, Suppression of host luminescence in the Pr:LuAG scintillator, IEEE Trans. Nucl. Sci. **55**, 1197 (2008).

[7] Y. Zorenko, A. Voloshinovskii, I. Konstankevych, V. Kolobanov, V. Mikhailin, and D. Spassky, Luminescence of excitons and antisite defects in the phosphors based on garnet compounds, Radiation Measurements **38**, 677 (2004).

[8] Y. Zorenko, A. Voloshinovskii, V. Savchyn, T. Voznyak, M. Nikl, K. Nejezchleb, V. Mikhailin, V. Kolobanov, and D. Spassky, Exciton and antisite defect-related luminescence in $Lu_3Al_5O_{12}$ and $Y_3Al_5O_{12}$ garnets, Phys. Status Solidi B **244**, 2180 (2007).

[9] Y. Zorenko, T. Zorenko, V. Gorbenko, B. Pavlyk, V. Laguta, M. Nikl, V. Kolobanov, and D. Spassky, Luminescence and ESR characteristics of γ-irradiated $Lu_3Al_5O_{12}$:Ce single crystalline film scintillators, Radiation Measurements **45**, 419 (2010).

[10] V. Babin, K. Blazek, A. Krasnikov, K. Nejezchleb, M. Nikl, T. Savikhina, and S. Zazubovich, Luminescence of undoped LuAG and YAG crystals, Phys. Status Solidi C **2**, 97 (2005).

[11] Y. Zorenko, V. Gorbenko, I. Konstankevych, A. Voloshinovskii, G. Stryganyuk, V. Mikhailin, V. Kolobanov, and D. Spassky, Single-crystalline films of Ce-doped YAG and LuAG phosphors: Advantages over bulk crystals analogues, J. Lumin. **114**, 85 (2005).

[12] M. Nikl, J. Pejchal, E. Mihóková, J. A. Mareš, H. Ogino, A. Yoshikawa, T. Fukuda, A. Vedda, and C. D'Ambrosio, Antisite defect-free $Lu_3(Ga_xAl_{1-x})_5O_{12}$:Pr scintillator, Appl. Phys. Lett. **88**, 141916 (2006).

[13] S. K. Yadav, B. P. Uberuaga, M. Nikl, C. Jiang, and C. R. Stanek, Band-Gap and Band-Edge Engineering of Multicomponent Garnet Scintillators from First Principles, Phys. Rev. Applied **4**, 054012 (2015).

[14] M. Fasoli, A. Vedda, M. Nikl, C. Jiang, B. P. Uberuaga, D. A. Andersson, K. J. McClellan, and C. R. Stanek, Band-gap engineering for removing shallow traps in rare-earth $Lu_3Al_5O_{12}$ garnet scintillators using Ga^{3+} doping, Phys. Rev. B **84**, 081102 (2011).

[15] M. Kobayashi, Y. Usuki, M. Ishii, T. Yazawa, K. Hara, M. Tanaka, M. Nikl, and K. Nitsch, Improvement in transmittance and decay time of $PbWO_4$ scintillating crystals by La-doping, Nucl. Instrum. Methods Phys. Res., Sect. A **399**, 261 (1997).

[16] S. Baccaro, P. Bohacek, B. Borgia, A. Cecilia, I. Dafinei, M. Diemoz, M. Ishii, O. Jarolimek, M. Kobayashi, M. Martini, M. Montecchi, M. Nikl, K. Nitsch, Y. Usuki, and A. Vedda, Influence of La^{3+}-doping on radiation hardness and thermoluminescence characteristics of $PbWO_4$, Phys. Status Solidi A **160**, R5 (1997).

[17] M. Nikl, K. Kamada, V. Babin, J. Pejchal, K. Pilarova, E. Mihóková, A. Beitlerova, K. Bartosiewicz, S. Kurosawa, and A. Yoshikawa, Defect engineering in Ce-doped aluminum garnet single crystal scintillators, Cryst. Growth Des. **14**, 4827 (2014).

[18] S. Liu, J. A. Mareš, X. Feng, A. Vedda, M. Fasoli, Y. Shi, H. Kou, A. Beitlerova, L. Wu, C. D'Ambrosio, Y. Pan, and M. Nikl, Towards bright and fast $Lu_3Al_5O_{12}$:Ce, Mg optical ceramics scintillators, Adv. Opt. Mater., doi: (2016).

[19] J. Chen, L. Zhang, and R. Zhu, Large size LYSO crystals for future high energy physics experiments, IEEE Trans. Nucl. Sci. **52**, 3133 (2005).

[20] A. N. Belsky, E. Auffray, P. Lecoq, C. Dujardin, N. Garnier, H. Canibano, C. Pedrini, and A. G. Petrosyan, Progress in the development of $LuAlO_3$ based scintillators, IEEE Trans. Nucl. Sci. **48**, 1095 (2001).

[21] K. Kamada, T. Yanagida, J. Pejchal, M. Nikl, T. Endo, K. Tsutumi, Y. Fujimoto, A. Fukabori, and A. Yoshikawa, Improvement of scintillation properties in Pr doped $Lu_3Al_5O_{12}$ scintillator by Ga and Y substitutions, IEEE Trans. Nucl. Sci. **59**, 2130 (2012).

[22] J. A. Mareš, M. Nikl, A. Beitlerova, P. Horodysky, K. Blazek, K. Bartos, and C. D'Ambrosio, Scintillation properties of Ce^{3+}- and Pr^{3+}-doped LuAG, YAG and mixed $Lu_xY_{1-x}AG$ garnet crystals, IEEE Trans. Nucl. Sci. **59**, 2120 (2012).

[23] W. Drozdowski, K. Brylew, A. J. Wojtowicz, J. Kisielewski, M. Świrkowicz, T. Łukasiewicz, J. T. M. de Haas, and P. Dorenbos, 33000 photons per MeV from mixed $(Lu_{0.75}Y_{0.25})_3Al_5O_{12}$:Pr scintillator crystals, Opt. Mater. Express **4**, 1207 (2014).

[24] W. Drozdowski, K. Brylew, M. E. Witkowski, A. Drewniak, Z. Masewicz, A. J. Wojtowicz, J. Kisielewski, and M. Świrkowicz, Effect of Lu-to-Y ratio and Mo coactivation on scintillation properties of LuYAG:Pr and LuAG:Pr,Mo crystals, Opt. Mater., DOI: 10.1016/j.optmat.2016.01.020 (2016).

[25] C. R. Stanek, K. J. McClellan, M. R. Levy, C. Milanese, and R. W. Grimes, The effect of intrinsic defects on garnet

scintillator performance, Nucl. Instrum. Methods Phys. Res., Sect. A **579**, 27 (2007).
[26] A. P. Patel, C. R. Stanek, and R. W. Grimes, Comparison of defect processes in $RE\mathrm{AlO}_3$ perovskites and $RE_3\mathrm{Al}_5\mathrm{O}_{12}$ garnets, Phys. Status Solidi B **250**, 1624 (2013).
[27] Y. Shen, Y. Shi, X. Feng, Y. Pan, J. Li, Y. Zeng, M. Nikl, A. Krasnikov, A. Vedda, and F. Moretti, The harmful effects of sintering aids in Pr:LuAG optical ceramic scintillator, J. Am. Ceram. Soc. **95**, 2130 (2012).
[28] Y. Shen, X. Feng, V. Babin, M. Nikl, A. Vedda, F. Moretti, E. Dell'Orto, Y. Pan, J. Li, and Y. Zeng, Fabrication and scintillation properties of highly transparent Pr:LuAG ceramics using Sc,La-based isovalent sintering aids, Ceram. Int. **39**, 5985 (2013).
[29] G. Kresse and J. Hafner, *Ab initio* molecular dynamics for liquid metals, Phys. Rev. B **47**, 558 (1993).
[30] P. E. Blöchl, Projector augmented-wave method, Phys. Rev. B **50**, 17953 (1994).
[31] G. Kresse and D. Joubert, From ultrasoft pseudopotentials to the projector augmented-wave method, Phys. Rev. B **59**, 1758 (1999).
[32] J. P. Perdew, K. Burke, and M. Ernzerhof, Generalized Gradient Approximation Made Simple, Phys. Rev. Lett. **77**, 3865 (1996).
[33] H. J. Monkhorst and J. D. Pack, Special points for Brillouin-zone integrations, Phys. Rev. B **13**, 5188 (1976).
[34] M. Nikl, H. Ogino, A. Krasnikov, A. Beitlerova, A. Yoshikawa, and T. Fukuda, Photo- and radioluminescence of Pr-doped $Lu_3Al_5O_{12}$ single crystal, Phys. Status Solidi A **202**, R4 (2005).
[35] J. Pejchal, M. Nikl, E. Mihóková, J. A. Mareš, A. Yoshikawa, H. Ogino, K. M. Schillemat, A. Krasnikov, A. Vedda, K. Nejezchleb, and V. Múčka, Pr^{3+}-doped complex oxide single crystal scintillators, J. Phys. D **42**, 055117 (2009).
[36] M. Nikl, E. Mihóková, J. Pejchal, A. Vedda, Y. Zorenko, and K. Nejezchleb, The antisite Lu_{Al} defect-related trap in $Lu_3Al_5O_{12}$:Ce single crystal, Phys. Status Solidi B **242**, R119 (2005).
[37] K. Blazek, A. Krasnikov, K. Nejezchleb, M. Nikl, T. Savikhina, and S. Zazubovich, Luminescence and defects creation in Ce^{3+}-doped $Lu_3Al_5O_{12}$ crystals, Phys. Status Solidi B **241**, 1134 (2004).
[38] C. Hu, S. Liu, Y. Shi, H. Kou, J. Li, Y. Pan, X. Feng, and Q. Liu, Antisite defects in nonstoichiometric $Lu_3Al_5O_{12}$:Ce ceramic scintillators, Phys. Status Solidi B **252**, 1993 (2015).
[39] K. V. Ivanovskikh, J. M. Ogiegło, A. Zych, C. R. Ronda, and A. Meijerink, Luminescence temperature quenching for Ce^{3+} and Pr^{3+} d-f emission in YAG and LuAG, ECS J. Solid State Sci. Technol. **2**, R3148 (2013).
[40] V. Bachmann, C. Ronda, and A. Meijerink, Temperature quenching of yellow Ce^{3+} luminescence in YAG:Ce, Chem. Mater. **21**, 2077 (2009).
[41] J. Ueda, K. Aishima, and S. Tanabe, Temperature and compositional dependence of optical and optoelectronic properties in Ce^{3+}-doped $Y_3Sc_2Al_{3-x}Ga_xO_{12}$ ($x = 0$, 1, 2, 3), Opt. Mater. **35**, 1952 (2013).
[42] C. W. Struck and W. H. Fonger, *Understanding Luminescence Spectra and Efficiency Using W_p and Related Functions* (Springer-Verlag, Berlin, 1991).
[43] W. M. Yen, M. Raukas, S. A. Basun, W. van Schaik, and U. Happek, Optical and photoconductive properties of cerium-doped crystalline solids, J. Lumin. **69**, 287 (1996).
[44] E. van der Kolk, S. A. Basun, G. F. Imbusch, and W. M. Yen, Temperature dependent spectroscopic studies of the electron delocalization dynamics of excited Ce ions in the wide band gap insulator, Lu_2SiO_5, Appl. Phys. Lett. **83**, 1740 (2003).
[45] M. Fasoli, A. Vedda, E. Mihóková, and M. Nikl, Optical methods for the evaluation of the thermal ionization barrier of lanthanide excited states in luminescent materials, Phys. Rev. B **85**, 085127 (2012).
[46] J. Ueda, P. Dorenbos, A. J. J. Bos, A. Meijerink, and S. Tanabe, Insight into the thermal quenching mechanism for $Y_3Al_5O_{12}:Ce^{3+}$ through thermoluminescence excitation spectroscopy, J. Phys. Chem. C **119**, 25003 (2015).
[47] M. Nikl, A. Vedda, M. Fasoli, I. Fontana, V. V. Laguta, E. Mihóková, J. Pejchal, J. Rosa, and K. Nejezchleb, Shallow traps and radiative recombination processes in $Lu_3Al_5O_{12}$:Ce:Ce single crystal scintillator, Phys. Rev. B **76**, 195121 (2007).
[48] A. Vedda, M. Martini, F. Meinardi, J. Chval, M. Dusek, J. A. Mareš, E. Mihóková, and M. Nikl, Tunneling process in thermally stimulated luminescence of mixed $Lu_xY_{1-X}AlO_3:Ce$ crystals, Phys. Rev. B **61**, 8081 (2000).
[49] A. Vedda, M. Nikl, M. Fasoli, E. Mihóková, J. Pejchal, M. Dusek, G. Ren, C. R. Stanek, K. J. McClellan, and D. D. Byler, Thermally stimulated tunneling in rare-earth-doped oxyorthosilicates, Phys. Rev. B **78**, 195123 (2008).
[50] S. W. S. McKeever, *Thermoluminescence of Solids*, Cambridge Solid State Science Series (Cambridge University Press, Cambridge, England, 1985).
[51] E. Del'Orto, M. Fasoli, G. Ren, and A. Vedda, Defect-driven radioluminescence sensitization in scintillators: The case of $Lu_2Si_2O_7$: Pr, J. Phys. Chem. C **117**, 20201 (2013).
[52] I. Veronese, C. De Mattia, M. Fasoli, N. Chiodini, M. C. Cantone, F. Moretti, C. Dujardin, and A. Vedda, Role of optical fiber drawing in radioluminescence hysteresis of Yb-doped silica, J. Phys. Chem. C **119**, 15572 (2015).
[53] F. Moretti, G. Patton, A. Belsky, M. Fasoli, A. Vedda, M. Trevisani, M. Bettinelli, and C. Dujardin, Radioluminescence sensitization in scintillators and phosphors: Trap engineering and modeling, J. Phys. Chem. C **118**, 9670 (2014).
[54] O. Sidletskiy, A. Vedda, M. Fasoli, S. Neicheva, and A. Gektin, Crystal Composition and Afterglow in Mixed Silicates: The Role of Melting Temperature, Phys. Rev. Applied **4**, 024009 (2015).
[55] A. B. Muñoz-García, E. Anglada, and L. Seijo, First-principles study of the structure and the electronic structure of yttrium aluminum garnet $Y_3Al_5O_{12}$, Int. J. Quantum Chem. **109**, 1991 (2009).
[56] B. Liu, M. Gu, X. Liu, S. Huang, and C. Ni, Formation energies of antisite defects in $Y_3Al_5O_{12}$: A first-principles study, Appl. Phys. Lett. **94**, 121910 (2009).
[57] Y. Xu and W. Y. Ching, Electronic structure of yttrium aluminum garnet ($Y_3Al_5O_{12}$), Phys. Rev. B **59**, 10530 (1999).
[58] F. Euler and J. A. Bruce, Oxygen coordinates of compounds with garnet structure, Acta Crystallogr. **19**, 971 (1965).

[59] P. Lecoq, Development of new scintillators for medical applications, Nucl. Instrum. Methods Phys. Res., Sect. A **809**, 130 (2016).

[60] J. M. Ogiegło, A. Katelnikovas, A. Zych, T. Jüstel, A. Meijerink, and C. R. Ronda, Luminescence and luminescence quenching in $Gd_3(Ga, Al)_5O_{12}$ scintillators doped with Ce^{3+}, J. Phys. Chem. A **117**, 2479 (2013).

[61] V. Jary, M. Nikl, S. Kurosawa, Y. Shoji, E. Mihokova, A. Beitlerova, G. P. Pazzi, and A. Yoshikawa, Luminescence characteristics of the Ce^{3+}-doped pyrosilicates: The case of La-admixed $Gd_2Si_2O_7$ single crystals, J. Phys. Chem. C **118**, 26521 (2014).

[62] K. Kamada, T. Endo, K. Tsutumi, T. Yanagida, Y. Fujimoto, A. Fukabori, A. Yoshikawa, J. Pejchal, and M. Nikl, Composition engineering in cerium-doped $(Lu, Gd)_3(Ga, Al)_5O_{12}$ single-crystal scintillators, Cryst. Growth Des. **11**, 4484 (2011).

[63] Y. Wu, G. Ren, D. Ding, F. Yang, and S. Pan, Effects of scandium on the bandgap and location of Ce^{3+} levels in $Lu_{1-x}Sc_xBO_3$:Ce scintillators, Appl. Phys. Lett. **100**, 021904 (2012).